Journal of Building Pathology and Rehabilitation (2024) 9:63
https://doi.org/10.1007/s41024-024-00413-7

RESEARCH ARTICLE

Effects of recycled scrap alumina on the physical and mechanical properties of calcium sulfo-aluminate cement products

Gaëlle Annick Nyonda Yanze[1,3] · Emmunuel Tiffo[1] · Achile Nana[2,3,4] · Elie Kamseu[3,5] · Florence Uphie Chinje[1]

Received: 17 January 2024 / Revised: 20 March 2024 / Accepted: 26 March 2024 / Published online: 12 April 2024

Abstract

This work aims to resolve the environmental problem caused by alumina scrap by studying the effects of its partial replacement on physical and mechanical properties of calcium sulfo-aluminate (CSA) cement products. To this effect, mixtures obtained from a partial replacement of bauxite with respectively 0, 10, 20, 30 and 40% of recycled alumina scrap were studied. After processing the various raw materials (bauxite, limestone and alumina scrap), they were mixed together, pressed at 2 MPa and heated at 1200 °C. The resulting clinkers were crushed and mixed with 15% of commercial gypsum to obtain the various CSA cement powders used to produce testing specimens. The raw materials as well as the synthesized products were characterized. Globally, it appears that the addition of 30% of alumina scrap enhances both physical and mechanical properties of CSA cement products. After 28 days, CSA cement products obtained with the addition of 30% of alumina scrap show a densified structure with the lowest porosity and the highest compressive strength (40 MPa) as compared to those obtained without addition. Also, the addition of 30% of alumina scrap enables to obtain CSA cement products endowed with short setting time (3 to 8 min) and containing greater amount of ye'elimite (54.54%) as compared to those obtained without addition (45.34%). Indeed, alumina scrap promotes the formation of ye'elimite which is progressively transformed into ettringite with curing time and thereby contributing for the hardening of specimens. Hence, the recycling and using of alumina scrap in certain amount (30%) to substitute bauxite during the synthesis of CSA cements, is a suitable process to obtain sustainable binders endowed with improved physical and mechanical properties. These CSA cements can be technologically used to produce mortars and concretes for the construction of bridges and other related civil engineering applications.

Keywords Alumina scrap · Calcium sulfo-aluminate · Physical and mechanical properties · Recycling · Synthesis

✉ Achile Nana
achilenana@yahoo.fr; a.yanz@yahoo.com

✉ Elie Kamseu
kamseuelie2001@yahoo.fr

[1] Applied Inorganic Chemistry Laboratory, Department of Inorganic Chemistry, Faculty of Science, University of Yaoundé I, P.O. Box 812, Yaoundé, Cameroon

[2] Research Unit of Noxious Chemistry and Environmental Engineering, Department of Chemistry, Faculty of Science, University of Dschang, P.O. Box 67, Dschang, Cameroon

[3] Local Materials Promotion Authority, MINRESI/MIPROMALO, P.O. Box 2396, Yaoundé, Nkolbikok, Cameroon

[4] Institute of Construction Materials, Technical University of Dresden, 01062 Dresden, Germany

[5] Department of Engineering "Enzo Ferrari", University of Modena and Reggio Emilia, Via Vivarelli, 10, Modena 41125, Italy

1 Introduction

Nowadays, the development of infrastructures that will sustain population growth is becoming more important worldwide [1]. For the manufacture of mortars and concretes, the main binder used remains the Ordinary Portland Cement (OPC). It is employed in building and construction sectors with high energy consumption and generates about 5–8% of worldwide carbon dioxide (CO_2) during its production process [2–4]. Therefore, the need to develop alternative eco-friendly binders endowed with low environmental impact as compared to OPC such as calcium sulfo-aluminate (CSA) cements remains a major challenge [5]. Indeed, as compared to OPC, CSA cement exhibits lower CO_2 emission during its production process and lower manufacturing temperature (1250–1350 °C) which is about 100 to 200 °C lower as compared to the OPC production process [6, 7], lower

energy required for the grinding process as well as more significant consumption of industrial by-products [7–9]. In addition, CSA cement products present excellent structural performances such as early development of high mechanical performances, low alkalinity, good dimensional stability and exceptional durability [6, 10–14], thereby enabling them to be used in several domains of applications such as self-leveling screeds, freeways pavement and airport runways where a fast setting is required [15].

However, CSA cements can be prepared by mixing various feedstock materials, such as bauxite, clays, limestone, gypsum, and industrial by-products [6, 16–18]. Cameroon possesses 1.8 billion tons of bauxite ores and 100.000 tons of limestone [19], which are still poorly valorized and can be suitably used as feedstock materials for the development of CSA cements, OPC clinkers, geopolymers, alkali-activated binders, ceramic products, refractory bricks for furnaces and other related tools and building materials [20]. Especially in the aluminum factory (Littoral region, Cameroon), 90.000 tons of aluminum are produced annually, and the refining process used to obtain metallic aluminum produces about 2-2.5 tons of waste for each ton of aluminum produced [21]. Most often, a small fraction of these wastes is employed to manufacture households and building tools and used as Supplementary Cementitious Materials (SCM) in the production of OPC cements [22]. Conversely, a considerable portion of this waste remains in landfills, responsible for cancer diseases observed among some factory workers and the environmental pollution (water, soil, and air) recorded in that area [23]. Therefore, the recycling and using of this alumina scrap as a replacement for Al_2O_3 to manufacture CSA cements can help to save approximately 85% of bauxite ores [24]. Additionally, the transformation of this solid alumina scrap into new items will be benefit on the economic plan by reducing the production cost of some products through the limitation of the use of raw natural resources.

Recently, several studies about the synthesis of CSA cements have been extensively revised. Ren et al. [25] reported that one of the main issues with the production of CSA cements is the high cost of raw materials, especially alumina sources such as natural bauxites. Indeed, due to the mining process used as well as the relatively high amount of Al_2O_3 contained in some bauxite ores, this requires special treatment, such as the grinding process, which significantly affects the final production cost of the as-obtained CSA cements. Due to that, several studies were done to find alternative sources of bauxite, limestone, and gypsum [23, 26, 27]. Therefore, alumina scrap or aluminum trash resulting from the refining process of bauxite, known as one of the most harmful wastes, appears as the best alumina source that can be used to replace bauxite during the synthesis of CSA cements [28].

Additionally, Shen et al. [26], Wang et al. [27] and Xu et al. [23], demonstrated that it was possible to replace natural bauxite with red mud, alumina scrap, marble sludge, plaster, ladle slag, and phosphor-gypsum during the production of CSA cements. Similarly, alumina powder resulting from the secondary aluminum manufacturing process and anodized mud from the production of anodized aluminum was used as partly or total replacement of bauxite in the production of CSA cements [29–31]. Singh et al. [32] showed that calcium sulfo-aluminate-alumino ferrite-rich cements from particular chalk waste from fertilizer plants can also be used as feedstock material [31]. Yang et al. [33] observed that pyrite cinder was suitable for partially replacing bauxite during the manufacturing of belt-ferro-aluminate cements. These previous studies had demonstrated the feasibility of using industrial scraps and by-products as feedstock materials to manufacture CSA cements. To our knowledge, very few data regarding the effects of alumina scrap on physical and mechanical properties of CSA cements are available to date.

Thus, this research aims to study the effects of recycled alumina scrap on physical and mechanical properties of calcium sulfo-aluminate cement products. So, recycling and using alumina scrap as a bauxite substitute appears to be a sustainable solution to reduce the production cost of CSA cements, thereby contributing to the preservation of both the environment and natural resources (bauxite ores). Depending on the initial raw materials (bauxite, alumina scrap, limestone and gypsum) and the synthesized products, samples were analyzed by XRF, XRD, FTIR spectroscopy and Environmental Scanning Electron Microscopy (ESEM) analyses whereas physical and mechanical properties were assessed.

2 Materials and experimental procedures

2.1 Materials

The bauxite denoted as HB was collected from Minim-Martap (Adamawa region, Cameroon) and used as alumina source whereas the limestone rock referenced as ML was collected from Mintom (South region, Cameroon) and used as calcium oxide source in this study [34, 35]. Additionally, the commercial gypsum (GC) supplied by the Tunisian company Markassy was used as sulfur trioxide source whereas alumina scrap powders (Als) provided by the Cameroonian company were also used as alumina source. Indeed, dried powders of HB used were pink whereas those of ML, GC and Als were white. All these raw materials were processed before being used as feedstock materials for the synthesis of calcium sulfo-aluminate (CSA) cements.

Table 1 Mix design of raw materials (% by mass) prepared for CSA cement clinkers

Formulations	HB	Als	ML	GC	Water
S0	50	00	35	15	15
S10	40	10	35	15	15
S20	30	20	35	15	15
S30	20	30	35	15	15
S40	10	40	35	15	15

2.2 Experimental procedures

The bauxite (HB) and limestone (ML) samples were oven-dried (GenLabPrime) at 105 °C for 48 h to remove moisture before being ground using a ball mill (MGS Sarl) to have a particle size of $\phi \leq 75$ µm. Additionally, GC and Als samples were sieved at the same particle size. All four raw materials were mixed toughly in various proportions in a Hobart mixer (M & O Model N50-G) for 5 min to obtain blended powders used to synthesize CSA cement clinkers. Therefore, each obtained blended powder was moistened with distilled water (15% by mass) for another 5 min, and the obtained mixture was pressed thanks to a hydraulic press (Euro Lab, model 25.011) with a load of 2 MPa into a cylindrical mold with a diameter of 23.0 ± 0.1 mm. The obtained samples were initially dried at 105 °C in an oven for 30 min and then calcined at 1200 °C for 4 h in a programmable electric furnace (Nabertherm S.A.S, Model LH 60/14) at the heating rate of 5 °C / min. However, the various compositions of raw meal were cooled naturally to allow the formation of different crystalline phases of clinker since these phases are usually formed during the holding time (1 h). The resulting mix design of raw materials was denoted respectively as S0, S10, S20, S30, and S40, as summarized in Table 1. Figure 1 presents the raw meal along with the calcined clinkers (C1, $C1Als^{10}$, $C1Als^{20}$, $C1Als^{30,}$ and $C1Als^{40}$) at 1200 °C. After that, each clinker (85 g) was ground and mixed with 15% by mass of commercial gypsum to optimize setting time and strength development [12] for 15 min using a ball mill and then sieved at $\phi \leq 75$ µm mesh-sifter in order to obtain cement powders. The resulting powders were used to prepare the CSA cement pastes to compare physical and mechanical properties at early on with the reference CSA cement (made with C1 cement).

Moreover, each obtained clinker was mixed in a Hobart mixer for 1 min (speed = 0.5) using a water/cement (w/c) ratio of 0.40 or 0.45 to obtain the CSA cement pastes. This difference observed in water variation was related to the addition of alumina scrap, which absorbs more than 0.5% of water compared to the reference cement pastes. Before molding, one fraction of the paste was collected and used to measure the setting time according to EN 196-3 standard [36] thanks to the Vicat apparatus, whereas another fraction (fresh paste; 30 g) was poured into PVC cylindrical molds (height: 40 mm; diameter: 20 mm) and then vibrated for 5 min on an electrical shaking table (M& O, type 202, No. 106) to remove entrapped air bubbles. During the hardening of pastes, the resulting testing specimens were firstly covered with a thin film of plastic to avoid evaporation. After 24 h, the obtained specimens were demoulded and cured in water at room temperature before being characterized.

The chemical analyses of different raw materials were done by X-ray fluorescence thanks to a Bruker S8 Tiger device, whereas the mineralogy of samples was followed by X-ray diffraction analysis thanks to an Advance Bruker D8 device. The patterns were recorded with the monochromator CuKα radiation (λ = 1.54 Å), operating at 45 kV and 40 mA with a scanning rate of 0.1 °/s in the 2θ range of 5–70 °. The crystalline phases were identified by comparing the obtained patterns with the Powder Diffraction File (PDF) standards from the International Centre for Diffraction Data (ICDD). Infrared spectroscopy analysis was done using a Nicolet 6700 FTIR spectrometer, and all spectra were recorded with a resolution of 4 cm^{-1} within the range of 4000–500 cm^{-1} in absorbance mode. The water absorption test was determined following ASTM C-642 standard [37], whereas the bulk density was measured by using Archimedes methods under ASTM C-20 standard [38] thanks to an electric balance (Ceramic Instrumentals, Sartorius model 1,712,001) endowed with a high sensitivity (± 0.001 g). The final value was the average of 3 tested specimens for each batch. The compressive strength of testing specimens initially cured at 25 ± 3 °C and immersed in tap water, was assessed using a hydro-electric press (Impact Test Equipment Limited, 250 KN) operating at a constant displacement rate of 0.500 MPa/s following EN 196-1 standard [32]. This test was performed on specimens aged 1, 3, 7, 14, and 28

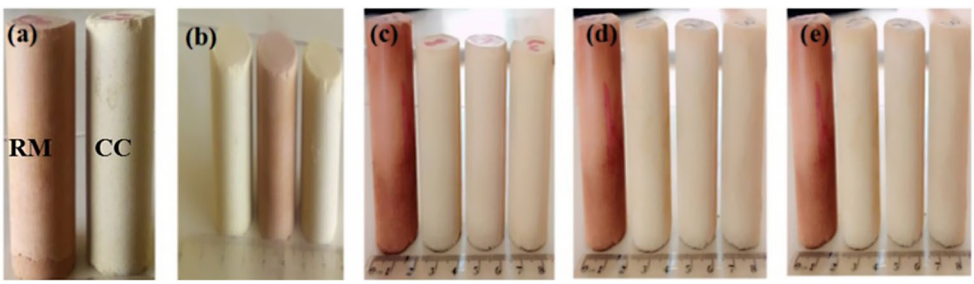

Fig. 1 Raw meal (RM) along with the calcined clinkers (CC): (a) C1, (b) $C1Als^{10}$, (c) $C1Als^{20}$, (d) $C1Als^{30}$ and (e) $C1Als^{40}$

Table 2 Chemical composition (wt%) of the starting materials (HB, ML, Als and GC) used

Composition	HB	ML	Als	GC
CaO	/	39.06	7.30	36.91
SiO_2	1.03	13.90	30.70	2.97
MgO	/	4.07	5.00	2.04
Al_2O_3	59.08	3.82	43.26	0.86
Fe_2O_3	5.12	2.04	4.46	0.35
K_2O	/	1.65	2.2	0.23
SO_3	0.04	0.43	0.80	45.25
TiO_2	3.61	0.19	0.90	/
SrO	/	0.19	/	0.50
P_2O_5	0.10	0.12	/	0.04
LOI[a]	30.87	34.33	5.38	10.78
Total	100.01	99.99	100.03	100.01

[a] loss on ignition at 1050 °C

days, respectively, and 3 replicate specimens of each batch were used for measurement. Additionally, the polished and etched surfaces of the resulting broken specimens after gold coating were analyzed using a FEI Quanta FEG 450 ESEM operating at 10 kV.

3 Results and discussion

3.1 Characterization of starting materials

The chemical compositions of HB, ML, GC, and Als samples are summarized in Table 2. It can be seen that bauxite (HB) contains 59.03% of aluminum oxide (Al_2O_3) and 43.20% of iron (III) oxide (Fe_2O_3) as major oxides. Also, it contains titanium oxide (TiO_2: 3.61%) and silicon oxide (SiO_2: 1.03%) appeared as minor oxides. This significant amount of Al_2O_3 enables HB to be considered as an alumina source material [39]. Indeed, this is due to the presence of alumina in the form of gibbsite ($Al(OH)_3$: PDF# 33–180), as confirmed by both the XRD pattern (Fig. 2) and FTIR spectrum of HB (Fig. 3) with the absorption bands of –OH groups of gibbsite appearing respectively at 3619, 3524, 3441 and 3366 cm^{-1} [40–42]. In addition, these absorption bands are attributed to the stretching vibrations of the hydroxyl group (O-H) of the gibbsite [40], whereas the one at 1014 cm^{-1} is attributed to the Si-O-Si stretching vibration, indicating the presence of silica [43]. As for those observed at 738 and 668 cm^{-1}, they are connected to the bending vibrations of O-H ($Al_{(VI)}$-OH) bonds of gibbsite [40, 44]. Additionally, a small amount of SiO_2 in the HB sample shows that the bauxite used can be classified as lateritic bauxite [45]. The XRD pattern of HB also indicates the presence of other minerals such as boehmite ((γ-AlO(OH): PDF# 21-1307), hematite (α-Fe_2O_3: PDF# 13–534), corundum (α-Al_2O_3: PDF# 10–173) and anatase (TiO_2: PDF# 71-1167).

Regarding alumina scrap (Als), it contains aluminum oxide (Al_2O_3: 43.26%), silicon oxide (SiO_2: 30.70%) and iron (III) oxide (Fe_2O_3: 4.46%) as major oxides, associated among others with calcium oxide (CaO: 7.30%), potassium oxide (K_2O: 2.2%) and magnesium oxide (MgO: 5.00%) as minor oxides. The presence of gibbsite, corundum and

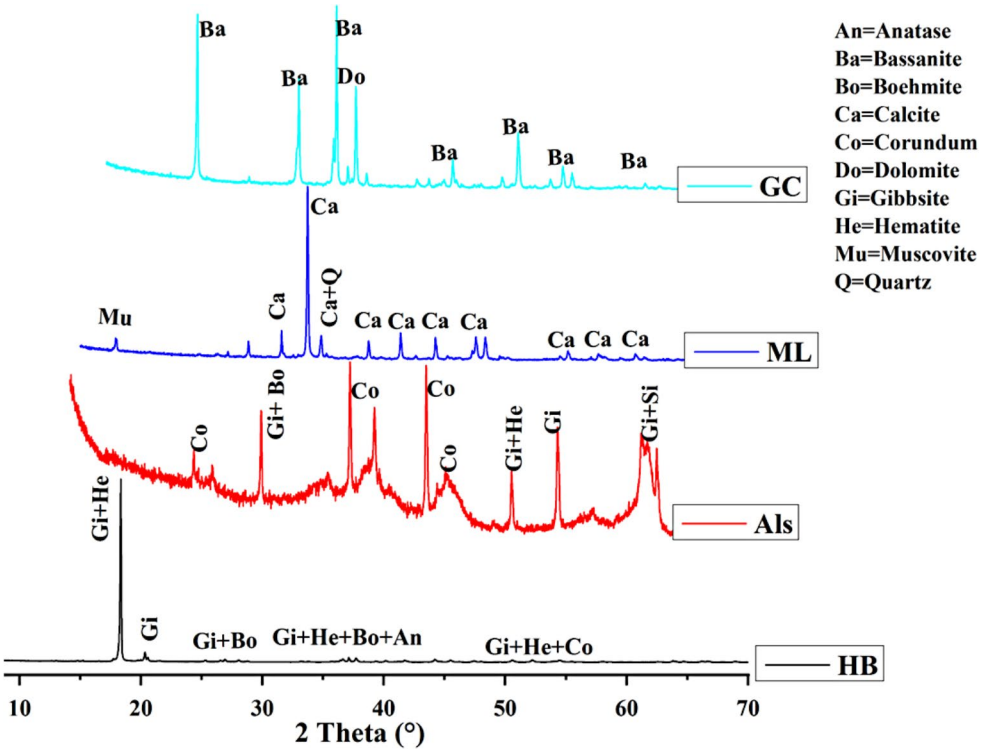

Fig. 2 XRD patterns of different raw materials

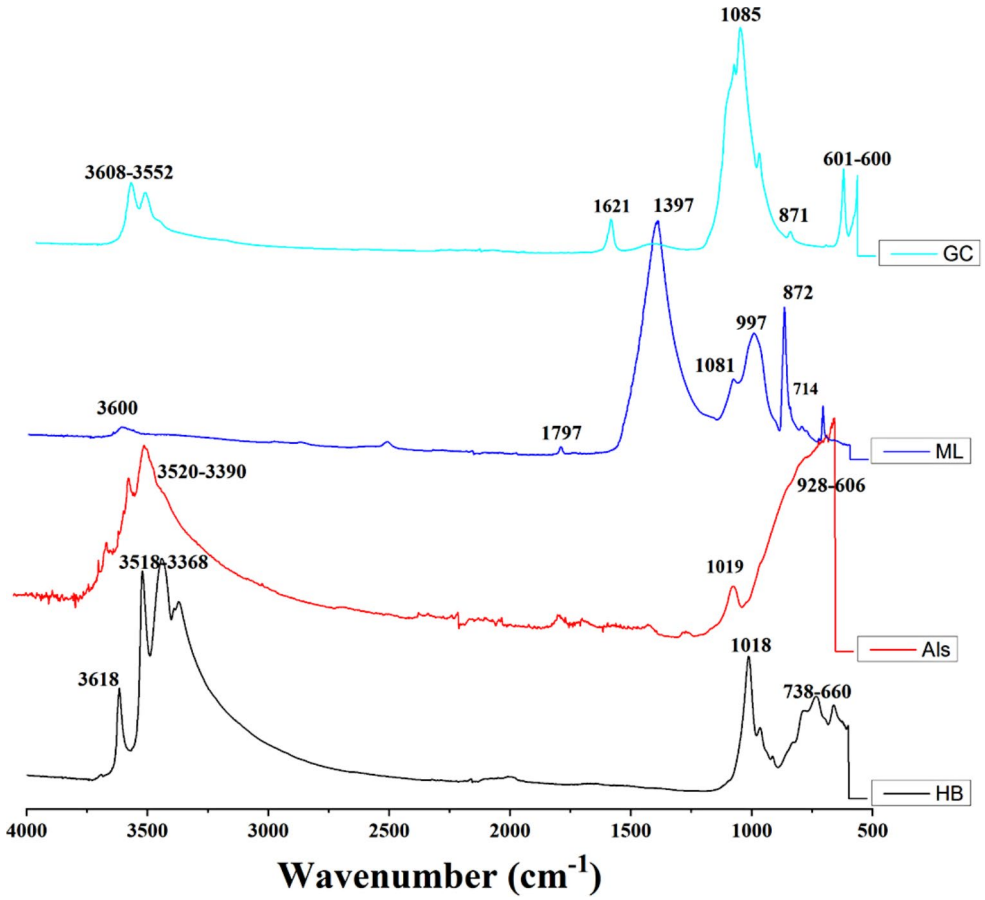

Fig. 3 FTIR spectra of raw materials

quartz is also confirmed by the XRD pattern (Fig. 2). The absorption bands of gibbsite (Als) appearing within the range of 1014–966 cm^{-1}, correspond to the O-H stretching modes of absorbed water molecules (Fig. 3) [46, 47]. The high amount of SiO_2 in the alumina scrap confirms the presence of non-crystallized kaolinite mineral (Fig. 2), which is highlighted on the IR spectrum (Fig. 3) by the absorption bands of disorder kaolinite at 3619 cm^{-1} [47]. Other absorption band observed at around 1077 cm^{-1} on the IR spectrum of Als is attributed to the symmetric bending vibration of Si-O [48] while the one at 2900 cm^{-1} is ascribed to the υC-H asymmetric stretching vibration and symmetric stretching vibration (υCH2) of organic impurities in Als. The high content of amorphous phase highlighted by a large dome observed in between 5 and 70° 2θ on the XRD pattern of Als (Fig. 2) suggests that it may enhance the rate of ye'elimite formation as previously reported by Liu et al. [49].

Concerning the limestone (ML), it contains 39.06% of CaO and 13.90% of SiO_2 as major oxides. Indeed, the presence of the abovementioned oxides is confirmed by the presence of calcite ($CaCO_3$: PDF# 5-586) and quartz (SiO_2: PDF# 46-1045) respectively on the XRD pattern (Fig. 2). Additionally, the absorption band (Fig. 3) at 2508 cm^{-1} is attributed to the C-O bond vibration of CO_2 [40, 44, 50], the one at 1797 cm^{-1} is connected to the internal vibration mode of the C = O bond of the carbonate group (CO_3^{2-}) [44], while those at 1397 and 872 cm^{-1} are respectively ascribed to the vibration mode of asymmetric stretching of C-O and in-plane bending vibration of the valence bonds O-C-O of the CO_3^{2-} group. The band at 714 cm^{-1} is characteristic of the out-of-plane bending vibration of O-C-O group [40, 50]. In the same way, the absorption band at 3600 cm^{-1} [41] is attributed to Si-O which is in accordance with the XRD results (Fig. 2).

Referring to the commercial gypsum (GC), it contains CaO (36.9%) and SO_3 (45.2%) as main oxides. However, CaO is mainly observed in dolomite ($CaMg(CO_3)_2$: PDF# 36–426) whereas SO_3 is found in bassanite ($CaSO_4.0.5H_2O$: PDF# 41–0224) as shown by the XRD pattern (Fig. 2). In addition, the absorption bands (Fig. 3) observed within the range of 3608–3552 cm^{-1} correspond to the stretching vibration modes of the O-H bonds of water molecules [48] while the band observed at 1621 cm^{-1} is attributed to the O-H bending vibration mode of bassanite [51]. Also, the band located at 1085 cm^{-1} corresponds to the S-O stretching vibration of sulfate group [52]. Finally, the bending vibration of the SO_4^{2-} tetrahedron of sulfate group appears within the range of 665 and 600 cm^{-1} [53]. The band located

at 871 cm^{-1} is characteristic of the out-of-plane bending vibration of the O-C-O of CO_3^{2-} group [40, 50]. Thus, these oxides can react together to give a cementitious phase such as ye'elimite ($C_3A_4\hat{S}$), responsible for strength development at the early age of CSA cements [54].

3.2 Characterization of synthesized CSA cements

3.2.1 Chemical compositions

The compositions obtained by XRF of different meal cements produced are summarized in Table 3. It can be observed that all formulations contain alumina (Al_2O_3), calcium oxide (CaO), silica (SiO_2) and sulfur trioxide (SO_3) as major oxides, associated, among others with magnesium oxide (MgO), Titanium oxide (TiO_2), potassium oxide (K_2O) and sodium oxide (Na_2O) as minor oxides. The content of alumina oxide increases with up to 30% of alumina scrap (Al_2O_3: 54.25%) addition and decreases with the addition of 40% (Al_2O_3:41.88%). The difference of about 12.37% observed is probably due to the fact that another fraction of alumina is transformed into α-Al_2O_3, known as corundum, responsible for the hardness of $C1Als^{30}$ cements. In addition, the presence of corundum in the cements is responsible for the formation of high amount of ye'elimite phase (54.54%) as confirmed by the XRD pattern of cements (Fig. 4). Thus, ye'elimite appears as the main phase of calcium sulfo-aluminate cements.

However, with the addition of 40% of alumina scrap (Als), the α-Al_2O_3 becomes unstable and creates high pores [55], then reducing the formation of alumina oxide and ye'elimite in the $C1Als^{40}$ sample as observed in Table 3. This corroborates with the study of Pereira et al. [49], who demonstrated that aluminum dross can be used as a partial replacement material for cements in certain limits to obtain environmental and economic advantages. Besides, the same observations were made for the belite (C_2S) and browmillerite (C_4AF) phases, which are also the secondary phases of calcium sulfo-aluminate cements [56]. Conversely, the addition of alumina scrap up to 30% reduces the CaO, MgO and TiO_2 contents and increases these contents after the addition 40%. The opposite effect is observed for both K_2O and Na_2O contents. This opposite effect is due to the fact that, alkalis affect the mineral composition, shape and size of phases [54–56] and consequently the hydration rate [57]. Indeed, the transformation of alumina into corundum enhances the physical and mechanical properties of cement products. The high MgO content observed can be attributed to the use of both limestone and alumina scrap with a MgO content ranging from 4 to 5% (Table 1). Regarding the estimation of mineralogical phases of clinkers, modified Bogue equations were adapted to the CaO-SiO_2-Al_2O_3-Fe_2O_3-SO_3

Table 3 Chemical composition of CSA cements along with the estimated theoretical Bogue mineralogical compositions

Formulations	Compositions (wt%)											
	SiO_2	Al_2O_3	Fe_2O_3	CaO	SO_3	MgO	K_2O	Na_2O	TiO_2	LOI[a]	C_4A_3S	C_2S	C_4AF
C1	7.80	45.89	4.66	25.65	6.84	2.32	0.73	0.08	2.70	2.89	45.34	23.36	14.18
$C1Als^{10}$	7.99	48.49	3.82	24.46	5.36	2.33	0.86	0.14	2.09	3.96	48.40	22.91	11.63
$C1Als^{20}$	7.41	51.48	3.02	23.85	5.44	2.30	0.81	0.16	1.54	3.63	51.39	21.25	9.19
$C1Als^{30}$	7.00	54.25	2.30	22.71	5.39	2.22	0.77	0.22	1.02	3.77	54.54	20.07	6.99
$C1Als^{40}$	8.03	41.88	4.48	26.81	9.38	2.53	0.85	0.08	2.56	2.88	40.80	23.02	13.63

[a]loss on ignition at 1050 °C

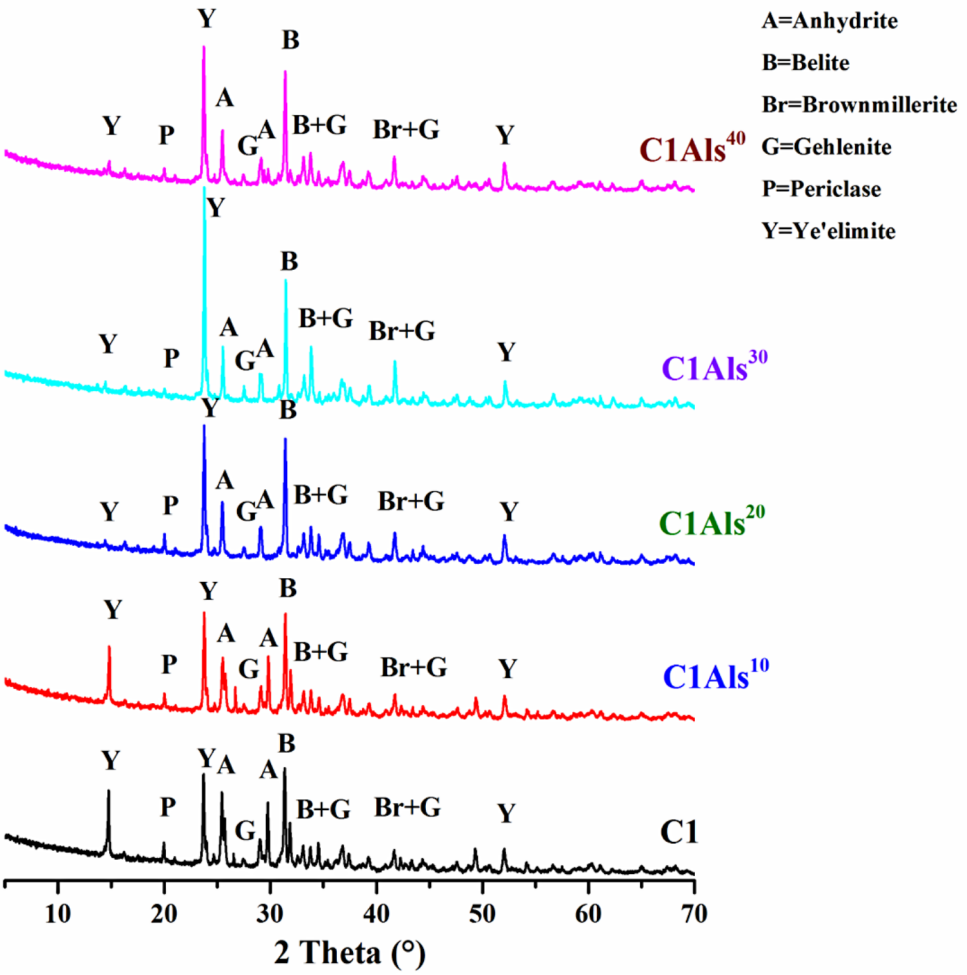

Fig. 4 XRD patterns of CSA cements

thermodynamic system [57]. The phases expected to be formed in all cements were ye'elimite (C_4A_3S), belite (C_2S) and brownmillerite (C_4AF). Thus, the formulas 1, 2 and 3 were used for the calculations (Table 3).

$$\%C_4AF = 3.0343\%Fe_2O_3 \quad (1)$$

$$\%C_4A_3S = 1.995\%Al_2O_3 - 1.273\%Fe_2O_3 \quad (2)$$

$$\%C_2S = 2.867\%SiO_2 \quad (3)$$

3.2.2 Mineralogy and evolution of phases

The XRD patterns of various samples thermally treated at 1200 °C are presented in Fig. 4. It can be observed that all specimens are composed of ye'elimite ($Ca_4Al_6O_{12}SO_4$: PDF# 33–0256), belite (β-C_2AS: PDF# 086–0398) and anhydrite ($CaSO_4$: PDF# 37-1496) as main crystalline phases and which are generally known as cementitious phases of CSA cements [31]. Indeed, anhydrite derives from the thermal transformation of bassanite whereas ye'elimite results from the thermal transformation of the mixture of bauxite (HB), alumina scrap (Als), limestone (ML) and gypsum (GC). The presence of an anhydrite phase observed in these CSA cements suggests that it is impossible to heat bassanite up to 1200 °C without losing its structural water. Indeed, during the heating process, bassanite ($CaSO_4$.1/2 H_2O) is transformed firstly into anhydrite III (soluble anhydrite) at 200 °C, secondly into anhydrite II at 800 °C and finally into anhydrite I at around ~ 1200 °C [58, 59]. In addition with the three main phases (ye'elimite, belite and anhydrite) observed, some appear as minor phases such as periclase (MgO: PDF# 45–0946) and brownmillerite (C_4AF: PDF# 071–0667). Regarding the XRD patterns of C1, $C1Als^{10}$, $C1Als^{20}$, $C1Als^{30}$ and $C1Als^{40}$ specimens (Fig. 4), it can be observed that the intensity of the prominent peaks of ye'elimite in between 25 and 30° 2θ increases up to 40% with the addition of alumina scrap (Als) with a slight deviation observed in the peak of $C1Als^{30}$ formulation. This can be explained by the fact that alumina scrap is highly reactive at this particular percentage. Thus, it is

almost consumed and its increases the content of ye'elimite formed. Additionally, the intensity of the peak of ye'elimite for $C1Als^{30}$ specimens at 23.67° 2θ is doubled as compared to those of $C1Als^{10}$ and $C1Als^{20}$. This is in accordance with the results of chemical compositions of CSA cements (Table 3). According to Gallardo-Heredia et al. [60–62], this change observed pertaining to the intensity of ye'elimite main peaks can be attributed to Al_2O_3 compound. So, as Al_2O_3 content increases up to 30% in the mixture, ye'elimite intensity also increases accordingly [61], showing that alumina scrap can increase the rate of formation of ye'elimite and instead decrease the one of belite.

3.3 Physical and mechanical properties of hardened CSA cement pastes

3.3.1 Setting time

Figure 5 shows the variation of initial (IS) and final (FS) setting times of fresh pastes cured at room temperature. It can be observed that the initial setting time decreases from 12 to 3 min with the increasing amount of Als from 0 to 30%. Conversely, this initial setting time increases slightly (7 min) with addition of 40% of Als. This is due to the fact that the addition of 30% of Als leads to a fast reaction and this enhance the reaction kinetic, thereby contributing to a fast hydration reaction of ye'elimite and a short initial setting time recorded accordingly. These results corroborate with those obtained previously by Li et al. [62], who demonstrated that the initial setting time of CSA pastes decreases when ye'elimite content increases (Fig. 4). Similarly, the final setting time decreases from 22 to 8 min with the increasing amount of Als. The different setting times obtained correlate with the Chinese standard, whose values vary from 25 to 180 min for rapid hardening of sulfoaluminate cements [63]. The lowest initial and final setting times were respectively 3 and 8 min for the $C1Als^{30}$ formulation. This shows that the addition of 30% of alumina scrap leads to a fast reaction and rapid formation of ye'elimite, and which could also induce the formation of both ettringite and monosulfate responsible for the short setting time observed. According to Bernado et al. [64], this decrease in setting time can be attributed to the formation of hydration products responsible of the initial structuring. Additionally, the presence of SO_4^{2-}Y Ca^{2+} ions contributes to neutralize their charges with those of Al^{3+} Y OH^- ions, enabling the precipitation of crystal hydration products. Hence, ettringite and calcium sulfate are therefore responsible for both setting and hardening as reported by Milena et al. [65]. Referring to Dovál et al. [66], the fast product formed could be due to the high water/solid mass ratio (0.45) with the reaction product of monosulfate besides ettringite, hydro garnet and gibbsite.

3.3.2 Compressive strength

The compressive strengths of hardened cement pastes after 1, 3, 7, 14 and 28 days of curing are presented in Fig. 6. It can be observed that the compressive strength of all specimens increases with the curing time. Indeed, the strength values for C1, $C1Als^{10}$, $C1Als^{20}$, $C1Als^{30}$ and $C1Als^{40}$ specimens are respectively 10.5, 14.4, 17.5, 18.3 and 15.9 MPa

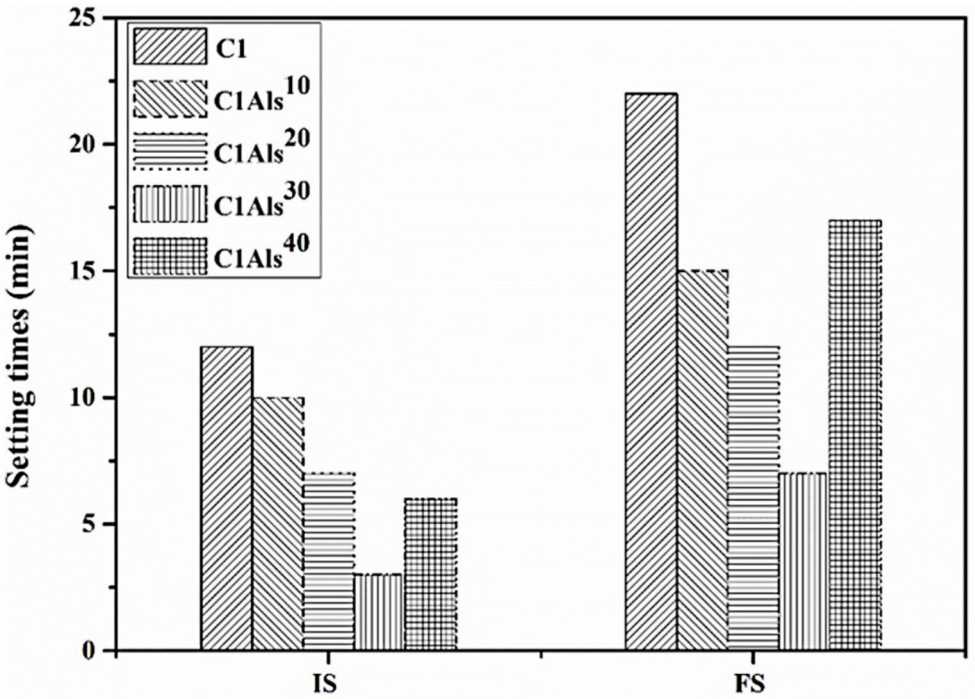

Fig. 5 Setting time of various fresh CSA cement pastes

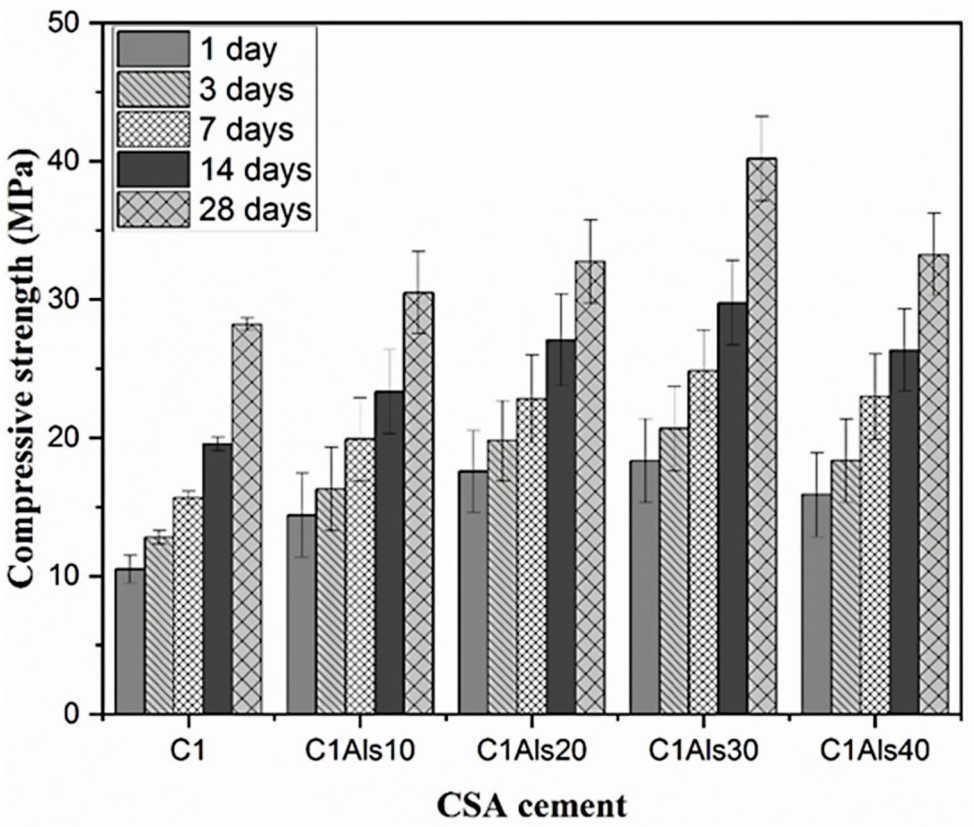

Fig. 6 Compressive strength of various hardened CSA cement pastes

after one day. In addition, these values are improved from 38 to 75%, 27 to 62%, 27 to 59%, 19 to 52% and 8 to 17% respectively after 28 days. Thus, the addition from 10 to 40% of Als provides supplementary reactive phases which contribute to produce cementitious matrices. Therefore, these matrices enhance the compactness and the hardness of the resulting structure which significantly improve the compressive strengths of specimens. It can be noticed that the addition of 40% of Als leads to decrease the compressive strength moderately of about 10% for the $C1Als^{40}$ specimens. This is can be attributed to the high amount Al_2O_3 resulting from Als and bauxite as well as limestone and gypsum released during cement hydration, which forms high content of belite responsible for low-strength development recorded. Additionally, the decrease of strength observed can also be assigned to the presence of non-reactive Als considered as an impurity inside the structure. The highest compressive strength value obtained with the addition of 30% of Als can be attributed to the formation of greater amount of ettringite phase in the structure (see formula 5). Indeed, CSA cements obtained with the addition of 30% of Als show highest compressive strengths at all ages. In addition, all CSA cement specimens exhibit enhanced compressive strength with curing time. This increase can be ascribed to the presence of aluminum in the structure, which inhibits cement hydration by forming metastable hydrated phases of monosulfate at early age. With time, these phases are transformed into more stable phases of ettringite (Formulas 4 and 5), thereby favoring the hardening of resulting CSA cement specimens [67, 68].

$$C_4A_3S + 18H \longrightarrow C_6AS_3H_{12} + 2AH_3 \quad (4)$$

$$C_4A_3S + 2CSH_2 + 34H \longrightarrow C_6AS_3H_{32} + 2AH_3 \quad (5)$$

3.3.3 Water absorption and bulk density

After compressive strength tests, both water absorption and bulk density versus curing time were carried out on two selected hardened CSA cement specimens (C1 and $C1Als^{30}$) and the results are summarized in Table 4. It can be observed that the water absorption increases with the curing time and decreases with the addition of alumina scrap (Als). Globally, the water absorption of the $C1Als^{30}$ specimens is lower as compared to that of C1 specimens. This is due to the low porosity developed along with the strengthening of cement matrix as result of the addition of Als. This in accordance with compressive strength results observed (Fig. 6). Conversely, the opposite effect was observed with bulk density at the same curing condition. So, the values recorded are 1.6 and 1.7 $Kg.m^{-3}$ for the C1 specimens, 1.7 and 1.8 $Kg.m^{-3}$

Table 4 Water absorption and bulk density of selected specimens initially fired at 1200 °C

Parameters	Formulations									
	C1					$C1Als^{30}$				
Curing time (days)	**1**	**3**	**7**	**14**	**28**	**1**	**3**	**7**	**14**	**28**
Water absorption (%)	15.2	18.3	23.7	25.8	14.7	12.9	20.7	14.2	29.8	12.2
Bulk density ($Kg.m^{-3}$)	1.7	1.7	1.6	1.6	1.7	1.7	1.7	1.8	1.8	1.8

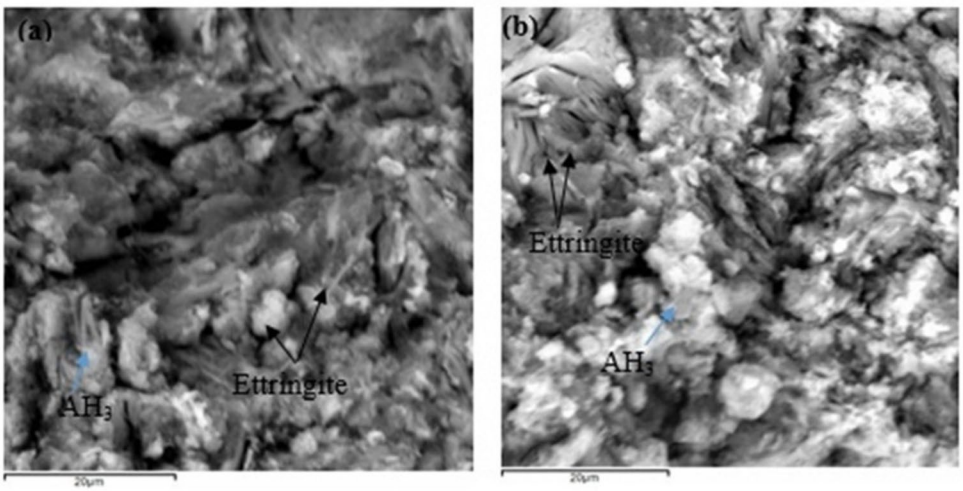

Fig. 7 ESEM images of hardened CSA cement specimens C1 and $C1Als^{30}$

for the $C1Als^{30}$ specimens respectively at 1, 3, 7,14 and 28 days. It can be noted that specimens with the highest compressive strength present the highest bulk density. This is because the more the structure is densified along with high compactness, the higher the resulting compressive strength.

3.3.4 Microstructure

Figure 7 shows the micrographs of the CSA cement specimens C1 and $C1Als^{30}$ aged 28 days. It can be observed that both the C1 and $C1Als^{30}$ specimens exhibit heterogeneous features. As for the C1 specimen (Fig. 7a), it appears less dense, showing visible cracks and voids along its surface and this in accordance with the low value of compressive strength recorded (Fig. 6). Additionally, the presence of ettringite is likely confirmed by the appearance of needle-shape crystals observed within the micrograph (Fig. 7a). Pertaining to the $C1Als^{30}$ specimen (Fig. 7b), it appears slightly homogeneous and dense as compared to the micrograph of C1 specimen, showing few cracks and visible voids. This account for the improved compressive strength previously recorded (Fig. 6). This shows that the excess alumina scrap content, which has not participated to the formation of ettringite, contributes to strengthen the structure so as to obtain few accessible voids. Hence, the $C1Als^{30}$ specimen contains greater amount of ettringite as compared to that of the C1 specimen. Thus, replacing C1 with up to 30% of alumina scrap is beneficial to form the ettringite phase, which improved and densified the structure in the $C1Als^{30}$ specimen than in the C1 specimen. However, in both formulations (C1 and $C1Als^{30}$), ettringite crystals are surrounded by some non-hydrated particles and amorphous hydration products that could be considered as aluminate hydroxide hydrate (AH_3). Similarly, the spongy-like features (Fig. 7a and b) can be attributed to ye'elimite with ettringite formed within its pores. This correlates with the study of El-Alfi et al. [31], who demonstrated that the sponge-like sulfo-aluminate phases are observed in the whole matrix whereas the needle-shape ettringite phases are found in the voids after 28 days of hydration.

4 Conclusion

This work has studied the effects of recycled alumina scrap on physical and mechanical properties of calcium sulfo-aluminate cements when used as partial replacement. The following conclusions could be drawn:

1. The additions of 0 up to 40% of alumina scrap increases the amount of ye'elimite in the as-obtained products with a maximum achieved with the addition of by 30%;
2. The setting times of all CSA cement pastes produced vary from 3 to 23 min due to the precipitation of crystalline hydration products such as ye'elimite;
3. The compressive strengths of all hardened CSA cement pastes vary from 15 to 40 MPa. Indeed, the addition of 30% of alumina scrap enables to obtain products

having the highest compressive strength (40 MPa) and short setting time (3 to 8 min) due to the high content of ye'elimite formed;
4. The addition of 30% of alumina scrap leads to CSA cement products having a densified structure, high compactness and low porosity as compared to the specimens obtained without addition;
5. CSA cement pastes obtained with the addition 30% of alumina scrap, as results of their improved physical and mechanical properties with curing time, can be technologically used as binders for the production of mortars and concretes, used for the construction of bridges and other related civil engineering applications.

Acknowledgements This project was funded by the Enterprise Group Comos through Mr. Timmamo Fokoua Victor, the European Union through the financial contribution N°PRICNAC-EEPER: MD2022, and the Institut de la Francophonie pour le developpement durable (IFDD/Canada)/Projet de Deployment des Technologies et Innovations Environnementales funded the Organisation International de la Francophonie (OIF). The authors wish to gratefully acknowledge the Ceramics & Glass Laboratory staff of the University of Trento, Italy, for their assistance in the characterization of samples.

Author contributions G.A.N.Y. Conceptualization, Methodology, Investigation, Writing - original draft. E.T. Writing - review & editing. A.N. Writing - review & editing, Investigation - original draft. E.K. Writing - review & editing. F.U.C. Writing - review & editing.

Funding The European Union through the financial contribution N°PRICNAC-EEPER: MD2022, and the Institut de la Francophonie pour le developpement durable (IFDD/Canada)/Projet de Deployment des Technologies et Innovations Environnementales funded the Organisation International de la Francophonie (OIF).

Data availability The data that supports this research is available but is not available to the public because it is confidential and is only used for this research.

Declarations

Conflict of interest The authors have no relevant financial or non-financial interests to disclose.

References

1. Tiffo E, Désiré P, Belibi B, Batiste J, Mbah B, Thamer A, Ebenizer T, Baenla J, Elimbi A (2021) Effect of various amounts of aluminium oxy-hydroxide coupled with thermal treatment on the performance of alkali-activated metakaolin and volcanic scor. Sci Afr 14:e01015. https://doi.org/10.1016/j.sciaf.2021.e01015
2. Idriss E, Tome S, Kamwa T, Aurelie R, Nana A, Deutou JG, Chongouang N, Alex J, Markus S, Christoph NAF, Etoh MA (2022) Engineering and structural properties of compressed earth blocks (CEB) stabilized with a calcined clay-based alkali-activated binder. Innov Infrastruct Solut 1–9. https://doi.org/10.1007/s41062-022-00760-9
3. Scrivener KL, Kirkpatrick RJ (2008) Innovation in use and research on cementitious material. 38:128–136. https://doi.org/10.1016/j.cemconres.2007.09.025
4. Gartner E (2010) Industrially interesting approaches to low-CO_2 cements. Cem Concr Res 34:1489–1498. https://doi.org/10.1016/j.cemconres.2004.01.021
5. Chaunsali P, Mondal P (2015) Influence of calcium sulfoaluminate (CSA) cement content on expansion and hydration behavior of various ordinary Portland cement-CSA blends. 2624. https://doi.org/10.1111/jace.13645
6. Hargis CW, Paula A, Monteiro PJM, Gartner EM (2013) Early age hydration of calcium sulfoaluminate (synthetic ye'elimite, C4A3S) in the presence of gypsum and varying amounts of calcium hydroxide Gypsum. Cem Concr Res 48:105–115. https://doi.org/10.1016/j.cemconres.2013.03.001
7. Aranda MAG, Santacruz I, De Torre AG, Londono-zuluaga D, Tob JI (2017) Clinkering and hydration of belite-alite-ye elimite cement. Cem Concr Compos 80:333–341. https://doi.org/10.1016/j.cemconcomp.2017.04.002
8. Zhou Q, Milestone NB, Hayes M (2006) An alternative to Portland Cement for waste encapsulation - the calcium sulfoaluminate cement system. J Hazard Mater 136:120–129. https://doi.org/10.1016/j.jhazmat.2005.11.038
9. Shi C, Jiménez AF, Palomo A (2011) New cements for the 21st century: the pursuit of an alternative to Portland cement. Cem Concr Res 41:750–763. https://doi.org/10.1016/j.cemconres.2011.03.016
10. Hanein T, Jose-Luis G-M, Bannerman MN (2017) Carbon footprint of calcium sulfoaluminate clinker production. J Clean Prod 2278–2287. https://doi.org/10.1016/j.jclepro.2017.11.183
11. Álvarez-pinazo G, Cuesta A, García-maté M, Santacruz I, Losilla ER (2012) Rietveld quantitative phase analysis of Yeelimite-containing cements. Cem Concr Res 42:960–971. https://doi.org/10.1016/j.cemconres.2012.03.018
12. Glasser FP, Zhang L (2001) High-performance cement matrices based on calcium sulfoaluminate – belite compositions. Cem Concr Res 31:1881–1886. https://doi.org/10.1016/S0008-8846(01)00649-4
13. Valenti GL, Marroccoli M, Pace ML, Telesca A, Chen IA, Hargis CW, Juenger MCG Reply to the discussion of the paper Understanding expansion in calcium sulfoaluminate-belite cements by, Valenti GL, Marroccoli M, Pace ML (2012) A. Telesca. Cem Concr Res 42:1560–1562. https://doi.org/10.1016/j.cemconres.2012.08.001
14. Ambroise J, Pe J (2004) New applications of calcium sulfoaluminate cement. Cem Concr Res 34:671–676. https://doi.org/10.1016/j.cemconres.2003.10.019
15. Chatterjee AK (1996) High belite cements-Present status and future technological options: part I. Cem Concr Res 26:1213–1225. https://doi.org/10.1016/0008-8846(96)00099-3
16. Li Y, Li J, Guo H (2015) Materials & Design Preparation and study of light transmitting properties of sulfoaluminate cement-based materials. Mater Des 83:185–192. https://doi.org/10.1016/j.matdes.2015.06.021
17. Shen Y, Qian J (2014) Utilisation of phosphogypsum for sulfate-rich belite sulfoaluminate cement production. Adv Cem Res 27:515–525. https://doi.org/10.1680/adcr.14.00071
18. Kim Y, Worrell E (2002) CO_2 emission trends in the cement industry: an international comparison. Mitig Adapt Strateg Glob Chang 7:115–133. https://doi.org/10.1023/A:1022857829028
19. Lemougna MP, Nzeukou NA, Billong N, Kamseu E, Desire T, Chinje U (2023) Materials engineering and local mineral resources for development in Cameroon J Mater Environ 14(02):14. ISSN: 2028–2508
20. Djobo YJN, Elimbi A, Dika Manga J, Djon Li Ndjock IB (2016) Partial replacement of volcanic ash by bauxite and calcined

oyster shell in the synthesis of volcanic ash-based geopolymers. Constr Build Mater 113:673–681. https://doi.org/10.1016/j.conbuildmat.2016.03.104
21. Tran H, Sorelli L, Ahmat O, Bouchard D, Brial V, Sanchez T, Conciatori D, Ouellet-plamondon C (2023) Development of sustainable ultra-high performance concrete recycling aluminum production waste. Constr Build Mater 371:130212. https://doi.org/10.1016/j.conbuildmat.2022.130212
22. Ulusu H, Aruntas HY, Kaplan G (2023) Mechanical, durability and microstructural characteristics of Portland pozzolan cement (PPC) produced with high volume pumice: Green, cleaner and sustainable cement development. Constr Build Mater 378:131070
23. Xu L, Wu K, Li N, Zhou X, Wang P (2017) Utilization of flue gas desulfurization gypsum for producing calcium sulfoaluminate cement. J Clean Prod 161:803–811. https://doi.org/10.1016/j.jclepro.2017.05.055
24. Liu W, Yang J, Xiao B (2009) Review on treatment and utilization of bauxite residues in China. Int J Min Process 93:220–231. https://doi.org/10.1016/j.minpro.2009.08.005
25. Ren C, Wang W, Li G (2017) Preparation of high-performance cementitious materials from industrial solid waste. Constr Build Mater 152:39–47. https://doi.org/10.1016/j.conbuildmat.2017.06.124
26. Shen Y, Qian J, Huang Y, Yang D (2015) Synthesis of belite sulfoaluminate-ternesite cements with phosphogypsum. Cem Concr Compos 63:67–75. https://doi.org/10.1016/j.cemconcomp.2015.09.003
27. Wang W, Wang X, Zhu J, Wang P, Ma C (2013) Experimental investigation and modeling of sulfoaluminate cement preparation using desulfurization gypsum and red mud. Ind Eng Chem Res 52:1261–1266. https://doi.org/10.1021/ie301364c
28. Kumar S, Kumar V, Prakash S (2021) Utilization of aluminium dross for the development of valuable product – a review. Mater Today Proc 43:547–550. https://doi.org/10.1016/j.matpr.2020.12.045
29. Wu K, Shi H, Guo X (2011) Utilization of municipal solid waste incineration fly ash for sulfoaluminate cement clinker production. Waste Manag 31:2001–2008. https://doi.org/10.1016/j.wasman.2011.04.022
30. Rafieizonooz M, Mirza J, Razman M, Warid M, Khankhaje E (2016) Investigation of coal bottom ash and fly ash in concrete as replacement for sand and cement. Constr Build Mater 116:15–24. https://doi.org/10.1016/j.conbuildmat.2016.04.080
31. El-Alfi RA, Gado EA (2016) Preparation of calcium sulfoaluminate-belite cement from marble sludge waste. Constr Build Mater 113:764–772. https://doi.org/10.1016/j.conbuildmat.2016.03.103
32. Singh M, Kapur PC (2008) Preparation of calcium sulphoaluminate cement using fertiliser plant wastes. J Hazard Mater 157:106–113. https://doi.org/10.1016/j.jhazmat.2007.12.117
33. Yang L, Yan Y, Hu Z, Xie X (2013) Utilization of phosphate fertilizer industry waste for belite – ferroaluminate cement production. Constr Build Mater 38:8–13. https://doi.org/10.1016/j.conbuildmat.2012.08.049
34. Fogue M, Anago GF, Fotsing BS, Ngnaguepa P, Fogue M, Anago GF, Fotsing BS, De PNL, Fogue M, Anago GF, Fotsing BS, Ngnaguepa P (2021) L'aluminium de récupération au service de l'alimentaire: fonderie et affinage (cas du Cameroun), Environnement. Ingénierie & Développement. 11:11–16. https://doi.org/10.4267/dechets-sciences-techniques.889
35. Philémon ZZ, Grelle MH, Philippe SA (2016) Physico-Chemical and Petrographic Characterization of Carbonated Rocks of Mintom (South-Cameroon) and their potential uses. Int J Geosci 7:775–783. https://doi.org/10.4236/ijg.2016.75059
36. Ruck L, Brown TC (2015) Setting time and 7-day strength of geopolymer mortar with various bindersQuantitative analysis of Munsell color data from archeological ceramics. J Archaeol Sci Rep 3:549–557. https://doi.org/10.1016/j.jasrep.2015.08.014
37. ASTM C642-21 (2022) Standard test method for density, absorption, and voids in hardened concrete. https://doi.org/10.1520/C0642-21
38. ASTM C20 (2010) Standard test methods for apparent porosity, water absorption, apparent specific gravity, and bulk density of burned refractory brick and shapes by boiling water. ASTM 1–3https://doi.org/10.1520/C0020-00R10.2.
39. Nyamsari DG, Yalcin MG (2017) Statistical analysis and source rock of the Minim-Martap plateau bauxite, Cameroon. Arab J Geosci 10:415–431. https://doi.org/10.1007/s12517-017-3172-0
40. Kloprogge JT, Ruan HD, Frost RL (2002) Thermal decomposition of bauxite minerals: infrared emission spectroscopy of gibbsite, boehmite and diaspore. J Mater Sci 37:1121–1129. https://doi.org/10.1023/A:1014303119055
41. Belinga R, Boum E, Rodrigue C, Juvenal K, Deutou G, Bakaine V, Nkwaju D, Rachel Y, Lemougna P, Francois N, Owono M, Kamseu E (2020) Thermal behaviour of metakaolin – bauxite blends geopolymer: microstructure and mechanical properties. SN Appl Sci. https://doi.org/10.1007/s42452-020-3138-9
42. Nana A, Tomé S, Anensong CSD, Venyite P, Djobo NJY, Ngouné J, Kamseu E, Bignozzi MC, Leonelli C (2022) Mechanical Performancee, Phase Evolution and Microstructure of Natural Feldspathic Solid solutions Consolidated Via Alkali activation: effect of NaOH concentration. Silicon 14:4107–4120. https://doi.org/10.1007/s12633-021-01193-2
43. Jordan MM, Sanfeliu T, de la Fuente C (2001) Firing transformations of Tertiary clays used in the manufacturing of ceramic tile bodies. Appl Clay Sci 20:87–95. https://doi.org/10.1016/S0169-1317(00)00044-2
44. Anand RR, Gilkes RJ, Roach (1991) Geochemical and mineralogical characteristics of bauxites, Darling Range, Western Australia. Appl Geochem 6(3):233–248. https://doi.org/10.1016/0883-2927(91)90001-6
45. Schellmann W (1994) Geochemical differentiation in laterite and bauxite formation. CATENA 21(1–2):131–143. https://doi.org/10.1016/0341-8162(94)90007-8
46. Nana A, Kamseu E, Akono A, Ngouné J (2021) Particles size and distribution on the improvement of the mechanical performance of high strength solid solution based inorganic polymer composites: a microstructural approach. Mater Chem Phys 267:124602. https://doi.org/10.1016/j.matchemphys.2021.124602
47. Tchakouté HK, Melele SJK, Djamen AT, Kaze CR, Kamseu E, Nanseu CNP, Leonelli C, Rüscher CH (2020) Microstructural and mechanical properties of poly(sialate-siloxo) networks obtained using metakaolins from kaolin and halloysite as aluminosilicate sources: a comparative study. Appl Clay Sci 186:105448. https://doi.org/10.1016/j.clay.2020.105448
48. Nana A, Alomayri TS, Venyite P, Kaze RC, Assaedi HS, Nobouassia CB, Valdès J, Sontia M, Ngouné J, Kamseu E, Leonelli C (2022) Mechanical properties and microstructure of a metakaolin-based Inorganic Polymer Mortar Reinforced with Quartz Sand, Silicon. 14:263–274. https://doi.org/10.1007/s12633-020-00816-4
49. Liu X, Li Y (2005) Effect of MgO on the composition and properties of alite-sulphoaluminate cement. Cem Concr Res 35:1685–1687. https://doi.org/10.1016/j.cemconres.2004.08.008
50. Nyamsari DG, Yalçin MG, Wolfson I (2020) Alteration, chemical processes, and parent rocks of Haléo-Danielle Plateau Bauxite, Adamawa–Cameroon. Lithol Min Resour 55:231–243. https://doi.org/10.1134/S0024490220030049
51. Juenger MCG, Winnefeld F, Provis JL, Ideker JH (2011) Advances in alternative cementitious binders. Cem Concr Res 41:1232–1243. https://doi.org/10.1016/j.cemconres.2010.11.012

52. Nana A, Sakue NE, Venyite P, Anensong CSD, Epey N, Adesoji AA, Kamseu E, Kumar S, Leonelli C (2024) Effect of milled pegmatite quarry wastes powders on structure, microstructure and mechanical properties of pegmatite-based geopolymers. Materialia 33:102022. https://doi.org/10.1016/j.mtla.2024.102022
53. Bolukbasi A, Kurt L, Palacio S (2016) Unravelling the mechanisms for plant survival on gypsum soils: an analysis of the chemical composition of gypsum plants from Turkey. Plant Biol 18:271–279. https://doi.org/10.1111/plb.12401
54. Luz CA, Rocha JC, Cheriaf M, Pera J (2006) Use of sulfoaluminate cement and bottom ash in the solidification/stabilization of galvanic sludge. J Hazard Mater 136:837–845. https://doi.org/10.1016/j.jhazmat.2006.01.020
55. Wang X, Liu G, Qi T, Huang W, Li X, Zhou Q (2021) Quantitative relationship between the density and structural unit of alpha alumina prepared from gibbsite and boehmite. Ceram Int 47:14464–14474. https://doi.org/10.1016/j.ceramint.2021.02.025
56. Winnefeld F, Lothenbach B, Dolenec S (2021) The influence of calcium sulfate content on the hydration of belite-calcium sulfoaluminate cements with different clinker phase compositions. Mater Struct 54:212–229. https://doi.org/10.1617/s11527-021-01811-w
57. Hanein T, Glasser FP, Bannerman MN (2020) Thermodynamic data for cement clinkering. Cem Concr Res 132:106043. https://doi.org/10.1016/j.cemconres.2020.106043
58. Rungchet A, Chindaprasirt P, Wansom S, Pimraksa K (2016) Hydrothermal synthesis of calciumsulfoaluminate-belite cement from industrial waste materials. J Clean Prod 115:273–283. https://doi.org/10.1016/j.jclepro.2015.12.068
59. Seufert S, Hesse H, Goetz-Neunhoeffer F, Neubauer J (2009) Quantitative determination of anhydrite III from dehydrated gypsum by XRD. Cem Concr Res 39(10):936–941. https://doi.org/10.1016/j.cemconres.2009.06.018
60. Gallardo-heredia M, Magallanes-rivera RX, Manuel J, Robles A-, Maldonado YG, Martínez-sánchez E (2021) Effect of temperature on the initial properties of calcium sulfoaluminate binders synthesised at 1100°C. Adv Apllied Ceram 120:240–247. https://doi.org/10.1080/17436753.2021.1945849
61. Pace ML, Telesca A, Marroccoli M, Valenti GL (2011) Use of industrial byproducts as alumina sources for the synthesis of calcium sulfoaluminate cements. Environ Sci Technol 45:6124–6128. https://doi.org/10.1021/es2005144
62. Li G, Zhang J, Song Z, Shi C, Zhang A (2018) Improvement of workability and early strength of calcium sulphoaluminate cement at various temperature by chemical admixtures. Constr Build Mater 160:427–439. https://doi.org/10.1016/j.conbuildmat.2017.11.076
63. Zhang L, Su M, Wang Y (1999) Development of the use of sulfo- and ferroaluminate cements in China. Adv Cem Res 11:15–21. https://doi.org/10.1680/adcr.1999.11.1.15
64. Bernardo G, Telesca A, Valenti GL (2006) A porosimetric study of calcium sulfoaluminate cement pastes cured at early ages. 36:1042–1047. https://doi.org/10.1016/j.cemconres.2006.02.014
65. Shakouri S, Erdo ST (2020) Laboratory production of calcium sulfoaluminate cements with high industrial waste content. Cem Concr Compos 106:103475. https://doi.org/10.1016/j.cemconcomp.2019.103475
66. Kumar M, Singh KS, Singh NP (2012) Heat evolution during the hydration of Portland cement in the presence of fly ash, calcium hydroxide and super plasticizer. Thermochim Acta 54:827–832. https://doi.org/10.1016/j.tca.2012.08.028
67. Ding J, Fu Y, Beaudoln JJ (1995) Strätlingite formation in high alumina cement-silica fume systems: significance of sodium ions. Cem Concr Res 25:1311–1319. https://doi.org/10.1016/0008-8846(95)00124-U
68. Radwan MM, Nagi SM (2022) Hydration behavior and formation of strätlingite compound (C_2ASH_8) in a bio-cement based on tricalcium silicate and mono-calcium aluminate for dental applications: influence of curing medium. Bull Natl Res Cent 46:180. https://doi.org/10.1186/s42269-022-00870-5